Electronic Supplementary Information

Synthesis of ZnO nanowire array within minutes

Experimental section

1. ZnO NWA synthesis

Zn nanocrystal coatings were electrodeposited at different current density (3, 6, 9 to 12 A dm^{-2}) from a sulfate bath consisted of zinc sulfate ($ZnSO_4 \cdot 7H_2O$, 100 g L^{-1}), boric acid (H_3BO_3, 20 g L^{-1}) and polyacrylamide [$(C_3H_5NO)_n$, 1 g L^{-1}] for 8 min. The experiments were carried out in a two-electrode cell with the conductive substrate (e.g., stainless steel mesh/sheet, nickel foam, carbon fiber paper, zinc, brass and copper sheets) and zinc plate as cathode and anode, respectively, at room temperature. The distance between cathode and anode was fixed at 2 cm. For the scalable experiment, the stainless steel mesh was chosen as substrate for electrodeposition of Zn nanocrystal coating, because of its low cost, good flexibility, easy to obtain and process. Subsequently, the ZnO NWAs can be grown from the Zn coatings via microwave hydrothermal treatment under different microwave power (280, 420, 560 and 700 W) and time (1, 2, 3 and 4 min) in an alkaline solution containing sodium hydroxide (NaOH, 10 g L^{-1}) and sodium citrate ($C_6H_5Na_3O_7 \cdot 2H_2O$, 20 g L^{-1}) without presence of any Zn source. The temperatures of hydrothermal solutions under different microwave power are approximate 70 °C (280 W), 96 °C (420 W), 96 °C (560 W) and 96 °C (700 W) respectively, measured by the thermometer. The microwave hydrothermal treatments were performed using a commercially available microwave oven (Midea, M1-211A) with polytetrafluoroethylene digestion tank. After these, the as-prepared samples were rinsed and dried immediately, then subjected to the structure and performance characterizations.

2. Characterization

2.1. Morphology and composition

Surface and cross-sectional morphology of Zn nanocrystal coating and ZnO nanowire array (ZnO NWA) was observed by scanning electron microscope (SEM, HITACHI SU8000). The grain size distribution of Zn coatings was determined by Nano Measure software, which was carried out by counting at least 50 points in the SEM images randomly, and then an average value was obtained through Gaussian fitting of the obtained data. The nano-structural characteristic, elemental composition and distribution of single ZnO nanowire were also studied by transmission electron microscopy (TEM, JEOL JEM-ARM200F) with energy dispersive X-ray spectroscopy (EDS, Zeiss ULTRA plus). The single ZnO nanowire was peeled off from the ZnO NWA via ultrasonic treatment in ethanol at a frequency of 40 kHz for 30 min. In addition, the Fourier transform infrared spectroscopy (FTIR, Thermo Fisher Scientific Nicolet iS50), Raman spectrometer (Jobin Yvon HR800), X-ray diffractometer (XRD, Rigaku UItima IV) and X-ray photoelectron spectroscopy (XPS, Thermo Scientific K-Alpha) were also employed to determine the chemical state, molecular and crystal structure of ZnO NWA.

2.2. Porosity

The structural characteristics of ZnO NWA, such as porosity, bulk density, apparent density, average pore diameter, median pore diameter, total intrusion volume and total pore area, were measured with a mercury intrusion porosimeter (Micromeritics, AutoPore V 9600).

2.3. Electrical resistance

The electrical resistance of Zn coatings grown on stainless steel sheet was evaluated by an AC Milliohm HiTester (Hioki 3541). Typically, 5 values were obtained for each sample, from which the average value was calculated.

2.4. Semiconductor type

Mott-Schottky measurement was performed in 0.5 M Na_2SO_4 solutions using an electrochemical workstation (Shanghai Chenhua, CHI 760E) with ZnO NWA grown on stainless steel mesh (area 1 × 1 cm^2), saturated calomel electrode (SCE) and platinum sheet (1 cm × 1 cm) as the working, reference and auxiliary electrode, respectively. The plots were obtained by using a 10 mV sine wave modulated signal with a constant step rate of 5 mV at different frequencies (e.g., 250, 500 and 750 Hz). After that, the semiconductor type of ZnO NWA can be determined by the slope of $C_{SC}^{-2} \sim E$ plot. The n-type and p-type semiconductor corresponds to the positive and negative slope, respectively, according to the following formulas [1]:

n-type:

$$C_{\mathrm{SC}}^{-2} = \frac{2}{\varepsilon\varepsilon_0 N_{\mathrm{d}}}(E - E_{\mathrm{fb}} - \frac{kT}{e}) \quad (1)$$

p-type:

$$C_{\mathrm{SC}}^{2} = -\frac{2}{\varepsilon\varepsilon_0 N_{\mathrm{a}}}(E - E_{\mathrm{fb}} - \frac{kT}{e}) \quad (2)$$

where C_{SC} is the capacitance, ε is the dielectric constant of ZnO (8.5), ε_0 is the vacuum permittivity (8.85×10^{-14} F cm^{-1}), N_d and N_a are the carrier concentrations, E is the applied potential, E_{fb} is the flat band potential, k is the Boltzman constant (1.38×10^{-23} J K^{-1}), T is the absolute temperature, and e is the elementary charge (1.602×10^{-19} C).

2.5. Optical property

The photoluminescence (PL, PerkinElmer LS-55) with He-Cd laser excitation (λ = 340 nm) and ultraviolet visible spectrophotometer (UV-vis, Hitachi U-3010) were used to evaluate the light emission and absorption performances of ZnO NWA grown on stainless steel mesh, respectively. Meanwhile, the bandgap (E_g, eV) can be calculated from the UV-vis spectrum, according the following equation [2]:

$$(\alpha hv)^2 = D(hv - E_g) \quad (3)$$

where α is optical absorption coefficient, hv is photon energy (eV), and D is constant.

2.6. Photoelectric response

The photoelectrochemical behavior of ZnO NWA grown on copper sheet (2 cm × 2 cm) in 0.5 M Na_2SO_4 solutions in darkness and under sunlight illumination was investigated in terms of photocurrent and electrochemical impedance spectra (EIS) measurements. Both of them were performed in the three-electrode cell controlled by CHI 760E workstation with platinum sheet, SCE and ZnO NWA as the auxiliary, reference and working electrode, respectively. The simulated sunlight source was provided by a 350 W Xe lamp (CEL-S350, Cel Sci-tech Co., Ltd.). The distance between the lamp and the electrode is 10 cm. Among them, the photocurrent curves were measured repeatedly over a period of 600 s under intermittent illumination. The EIS plots were conducted at open circuit potential with the alternating current amplitude of 10 mV and an applied frequency ranging from 10^{-2} Hz to 10^5 Hz.

2.7. Photocatalytic activity

The catalytic activity of ZnO NWA towards the photodegradation reaction of methyl orange (MO) and chromic oxide (Cr^{6+}) solutions was evaluated in a standard quartz cuvette (3.5 mL, 10 mm optical path) under ultraviolet irradiation provided by a 100 W ultraviolet lamp (Beijing Tianmai Henghui, GY250) as the optical source. Typically, 3 mL of MO or Cr^{6+} solutions (10 mg L^{-1}) and the ZnO NWA grown on stainless steel mesh (2 pieces, 1 cm^2 $piece^{-1}$) were sequentially added into the cuvette. After 30 min of standing period in dark to establish an adsorption-desorption equilibrium, the above system was placed under the ultraviolet light. And then an ultraviolet-visible spectrophotometer (UV-vis, Shanghai INESA Analytical N4) was used to monitor its absorbance variation, thereby calculating the reduction rate. All the tests were carried out at ambient conditions.

2.8. Catalytic hydrogenation

The catalytic activity of Cu nanoparticles with or without ZnO NWA supports towards the hydrogenation reaction of MO was also evaluated in the standard quartz cuvette. Typically, 3 mL of MO solutions (0.1 mM), 0.2 mL of freshly configured sodium borohydride ($NaBH_4$, 0.1 M) solutions, and the catalyst grown on stainless steel mesh (1 cm × 1 cm) were sequentially added into the cuvette. Then the INESA spectrophotometer was used to monitor the absorption spectrum of hydrogenation reaction. The ZnO NWA-supported Cu nanoparticles catalyst was synthesized via electrodeposition of Cu on the ZnO NWA. The electrodeposition process was performed in a pyrophosphate bath consisted of copper pyrophosphate ($Cu_2P_2O_7$, 132 g L^{-1}), potassium pyrophosphate ($K_4P_2O_7$, 330 g L^{-1}) and sorbitol ($C_6H_{14}O_6$, 7 g L^{-1}) under a potentiostatic condition of -0.3 V cm^{-2} for 20 s. In this regard, the platinum sheet and ZnO NWA were used as the anode and cathode respectively, while the other conditions including the electrolytic cell and temperature are the same as those of Zn electrodeposition.

Results and discussion

The surface morphology of ZnO NWAs grown from the NaOH solutions in the absence and presence of sodium citrate is shown in Figure S1. It can be seen that the latter (Figure S1b) with more homogeneous wire diameter distribution has smaller wire diameter and larger surface-to-volume ratio than those of ZnO NWA grown from the solutions without the additive (Figure S1a), indicating that the sodium citrate significantly improves the ZnO NWA's quality.

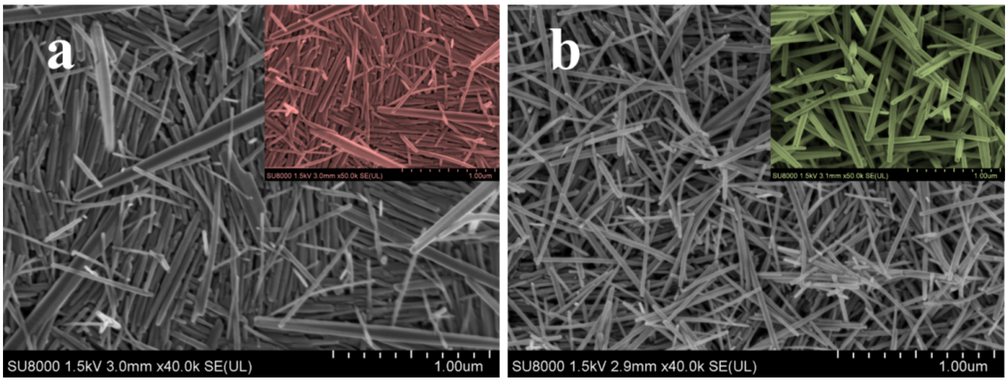

Figure S1. SEM images of ZnO NWAs grown from NaOH solutions in the absence (a) and presence (b) of sodium citrate, respectively.

Figures S2 and S3 display the surface and cross-sectional morphology of Zn coatings electrodeposited at different current density on the stainless steel meshes. It can be seen that the grain size of Zn coatings obtained at current density of 3, 6, 9 and 12 A dm^{-2} is approximate 25.33, 20.06, 13.59 and 10.98 nm, while the coating thickness is about 13.47, 17.50, 20.48 and 30.55 μm, respectively.

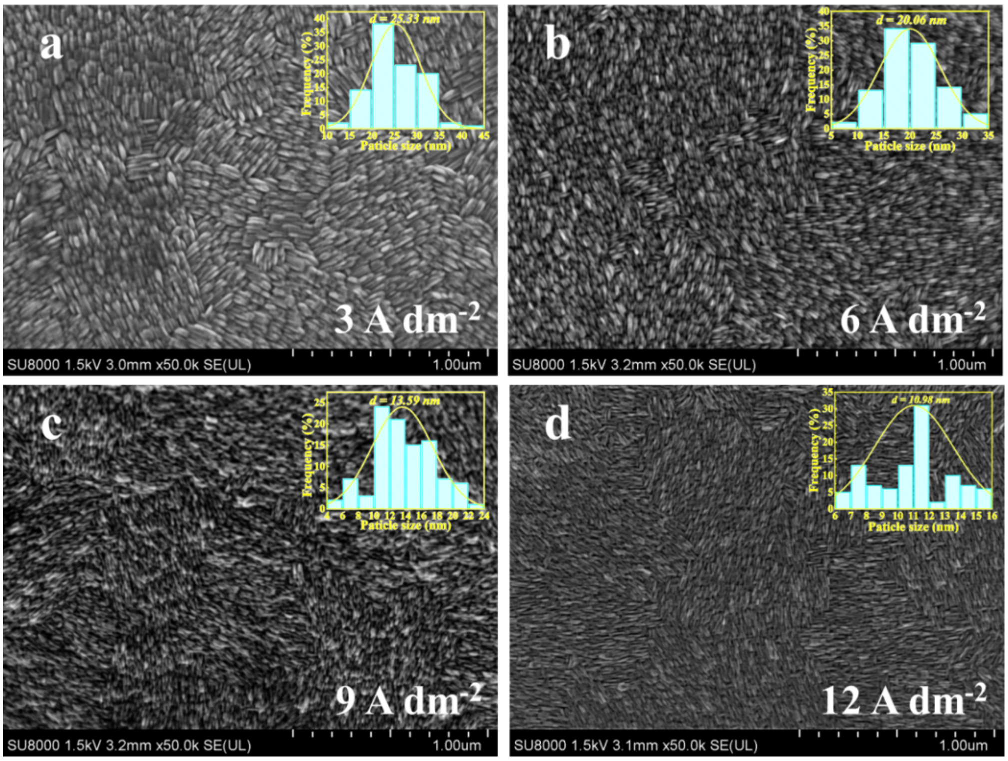

Figure S2. Surface SEM images along with the grain size distributions of Zn coatings electrodeposited at different current density.

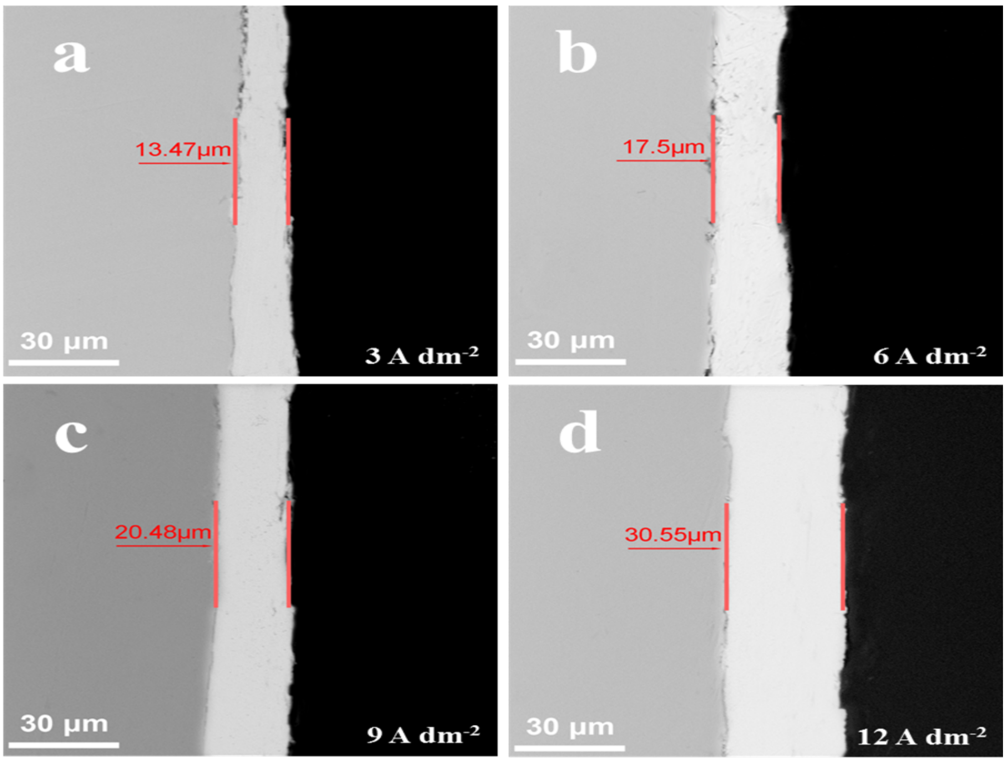

Figure S3. Cross-sectional SEM images of Zn coatings electrodeposited at different current density.

In order to further investigate the textural characteristics of ZnO NWA, the cumulative pore size distribution (CPSD) and differential pore size distribution (DPSD) were also measured, as presented in Figure S4. A summary of structural parameters was listed in Table S2. It can be seen that an obvious decrease in both CPSD (Figure S4a) and DPSD (Figure S4b) of stainless steel mesh with the growth of ZnO NWA, indicating the decreased porosity.

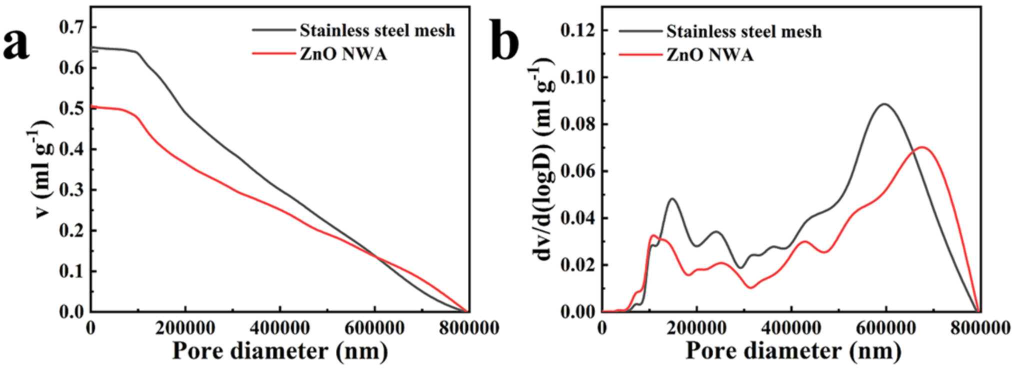

Figure S4. Cumulative pore size distribution (a) and differential pore size distribution (b) of the stainless steel mesh before and after coating with ZnO NWA.

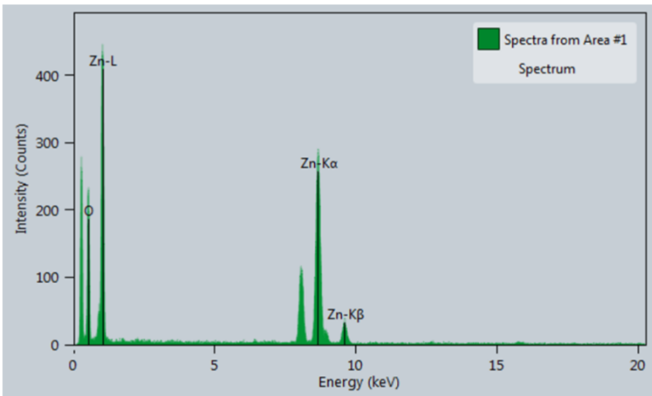

Figure S5. The EDS spectrum of single ZnO nanowire derived from Figure 2e.

The XPS test is performed to further confirm the chemical states of ZnO NWA. Figure S6 shows the XPS survey spectrum of ZnO NWA and corresponding high-resolution Zn 2p and O 1s spectra, respectively. As illustrated, a series of sharp signals correspond to the characteristic peaks of Zn 3d, Zn 3p, Zn 3s, Zn Auger, Zn 2p, O 1s, O Auger and C 1s, respectively, suggesting the existence of Zn, O and C elements (Figure S6a). Among them, the C element is probably derived from the hydrocarbon contaminants, due to the fact that the spectra are calibrated by the C 1s peak at the binding energy of

~284.8 eV. The characteristic peaks Zn 3d, 3p, 3s, $2p_{3/2}$ and $2p_{1/2}$ derived from ZnO NWA and inside Zn seed layer, are observed at ~9.7, ~88.3, ~139.5, ~1021.8 and ~1044.8 eV, respectively. It can be concluded that the Zn content mainly depends on the Zn $2p_{3/2}$ and $2p_{1/2}$ peaks according to their relatively high intensity. Noteworthy, there are no spin-orbit doublets in the high-resolution Zn 2p spectrum, indicating that the Zn mainly exists in the form of Zn^{2+} (Figure S6b). While the Zn and O Auger peaks may arise from the Zn bonded with O. Besides, the asymmetric O 1s peak can be fitted to two overlapping peaks located at ~530.2 eV (O_1) and ~531.2 eV (O_2), respectively. Among them, the O_1 peak is also attributed to the Zn-O bonds, while the O_2 peak is associated with O^{2-} ions that are in oxygen-deficient regions within the ZnO matrix (Figure S6c). The intensity of O_1 peak obviously exceeds that of the O_2 peak, suggesting the strong Zn-O bonding in ZnO NWA.

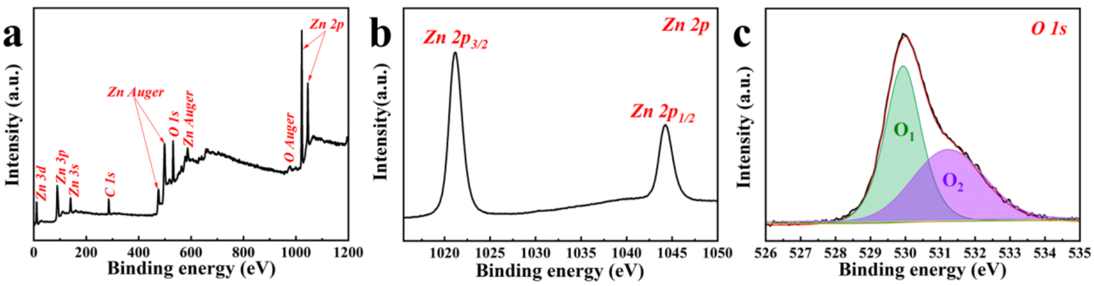

Figure S6. The XPS survey spectrum (a) and corresponding high-resolution Zn 2p (b) as well as O 1s (c) spectra of ZnO NWA.

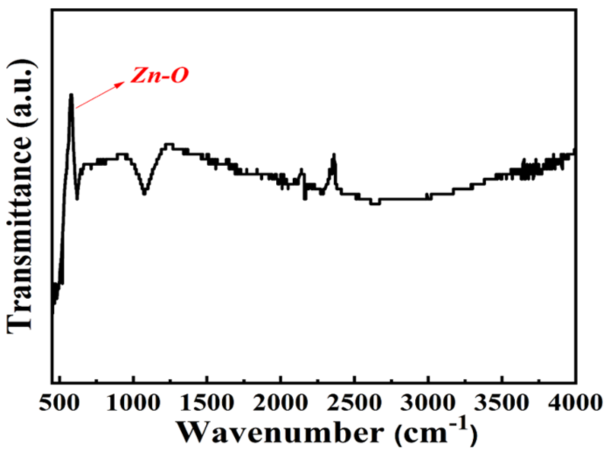

Figure S7. The FTIR spectrum of ZnO NWA.

Figure S8 exhibits the typical XRD spectrum of ZnO NWA grown from the Zn nanocrystal coating electrodeposited at 12 A dm^{-2} for 8 min under microwave power of 700 W for 2 min. As shown, the spectrum exhibits both characteristic peaks of ZnO and Zn, indicating that the sample consists of their mixed phases. Among them, the ZnO phase with preferred orientation along (101) plane is from the ZnO NWA, and the Zn phase may come from the inside Zn coating, because the ZnO NWA is still porous. In addition, Figures S9 and S10 also depict the XRD spectra of ZnO NWAs prepared at different microwave power and time, respectively. As shown, the diffraction peak intensity of ZnO is elevated with the enlargement of microwave power, while the microwave time has a similar effect on the ZnO's peak intensity, indicating the increase in crystallinity of ZnO NWA synthesized.

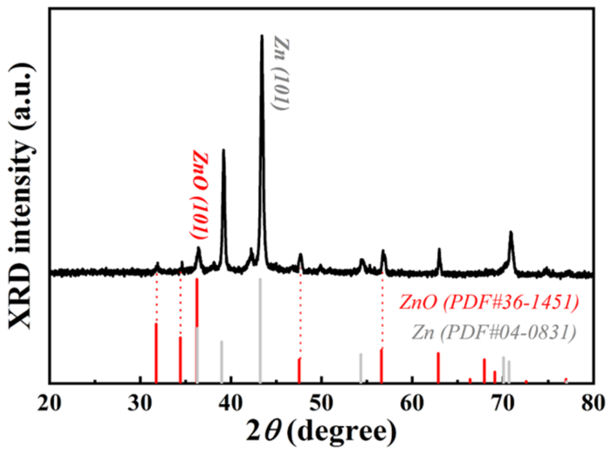

Figure S8. The XRD spectrum of ZnO NWA with the standard powder diffraction file (PDF) of Zn (PDF#04-0831) and ZnO (PDF#36-1451).

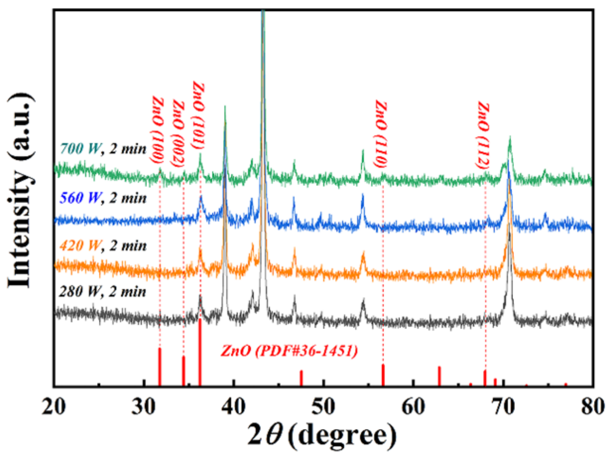

Figure S9. The XRD spectra of ZnO NWAs produced at different microwave power for 2 min.

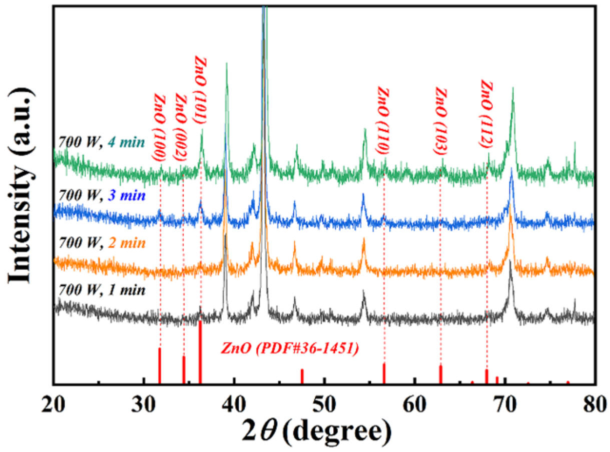

Figure S10. The XRD spectra of ZnO NWAs produced at a microwave power of 700 W for different time.

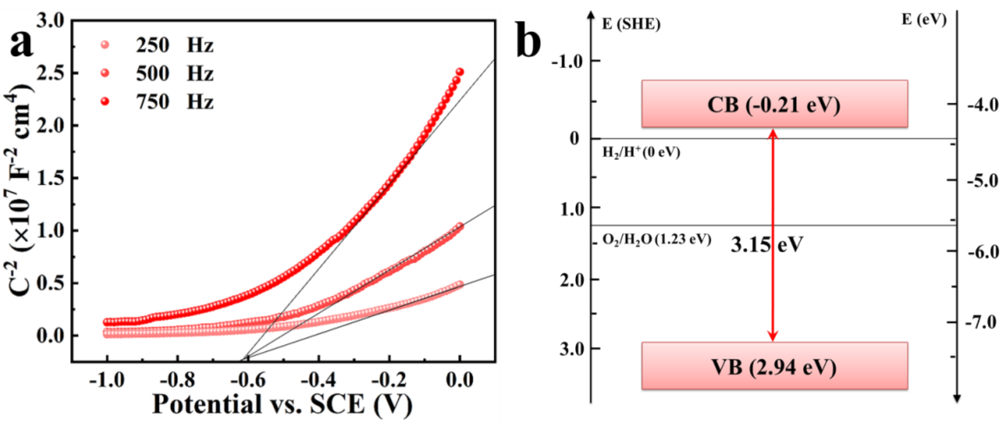

Figure S11. The Mott-Schottky plots at different frequencies (a) and a schematic illustration for the band structure (b) of ZnO NWA.

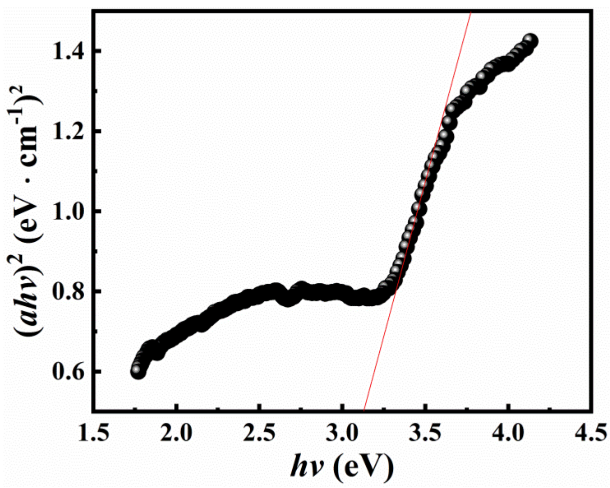

Figure S12. The Tauc's plot of ZnO NWA produced at a microwave power of 700 W for 2 min.

The charge transfer property of the as-prepared ZnO NWA was uncovered by the photoelectric chemistry measurements including chronoamperometry and electrochemical impedance spectroscopy (EIS). The photocurrent variation of ZnO NWA in 0.5 M Na_2SO_4 solutions under intermittent simulated sunlight illumination are shown in Figure S13a. It can be seen that the current density is significantly elevated under visible light irradiation compared to that in darkness, indicating that the light illumination gives rise to the effective separation of photo-generated electron-hole pairs. From the observation of EIS plots in Figure S13b, the decreased diameter of depressed capacitive semicircle also confirms the decreased charge transfer resistance and improved separation and immigration ability of electron-hole pairs when light illumination is added. These results demonstrate that the ZnO NWA possesses a certain photoelectric response to visible light, and thus it is expected to be a promising catalyst for photo-degradation treatment of industrial wastewater.

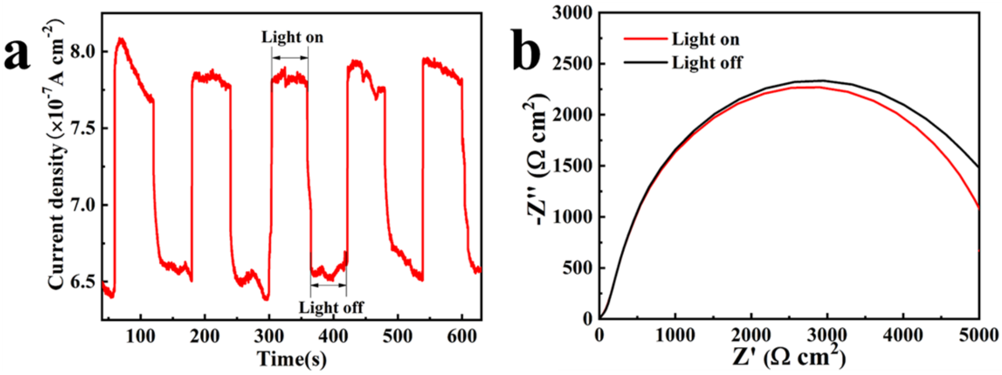

Figure S13. Photoelectric responses of ZnO NWA produced at a microwave power of 700 W for 2 min: (a) photocurrent and (b) EIS plots.

In order to verify the photocatalytic activity of ZnO NWA, its catalytic capacity towards the photo-degradation of methyl orange (MO) and hexavalent chromium ion (Cr^{6+}) under ultraviolet irradiation was examined. Figure S14 displays their UV-vis spectra during the photocatalytic reaction over ZnO NWA. It was clearly observed that the absorption peaks of MO and Cr^{6+} solutions were almost completely disappeared within 120 min and 90 min respectively, suggesting their full photo-degradation.

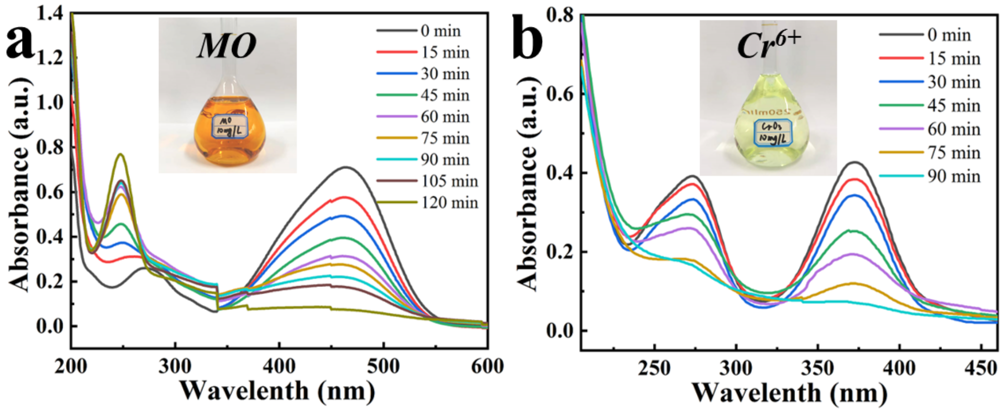

Figure S14. UV-vis absorption spectra during photocatalytic reaction of methyl orange (MO, a) and chromic oxide (Cr^{6+}, b) solutions over ZnO NWA produced at a microwave power of 700 W for 2 min.

In addition to the photocatalytic performances, the ZnO NWA can also be used as a support for other nano-catalysts, thereby producing the composite catalysts with array structure. Figures S15a and b exhibit the surface morphology of ZnO NWA before and after Cu electrodeposition, respectively. By comparing, it can be clearly seen that the Cu nanoparticles are homogeneously anchored on the ZnO NWA (Figure S15b). After that, the hydrogenation reaction of MO solutions over the ZnO NWA supported with and without Cu nanoparticles was also carried out to examine their catalytic activity. Figures S15c and d display their UV-vis spectra during the hydrogenation reaction, respectively. As shown, the ZnO NWA has almost no catalytic activity for the MO hydrogenation (Figure S15c), while the dye solutions are completely reduced within 210 s over the ZnO NWA-supported Cu nanoparticles catalyst (Figure S15d), indicating its outstanding catalytic activity.

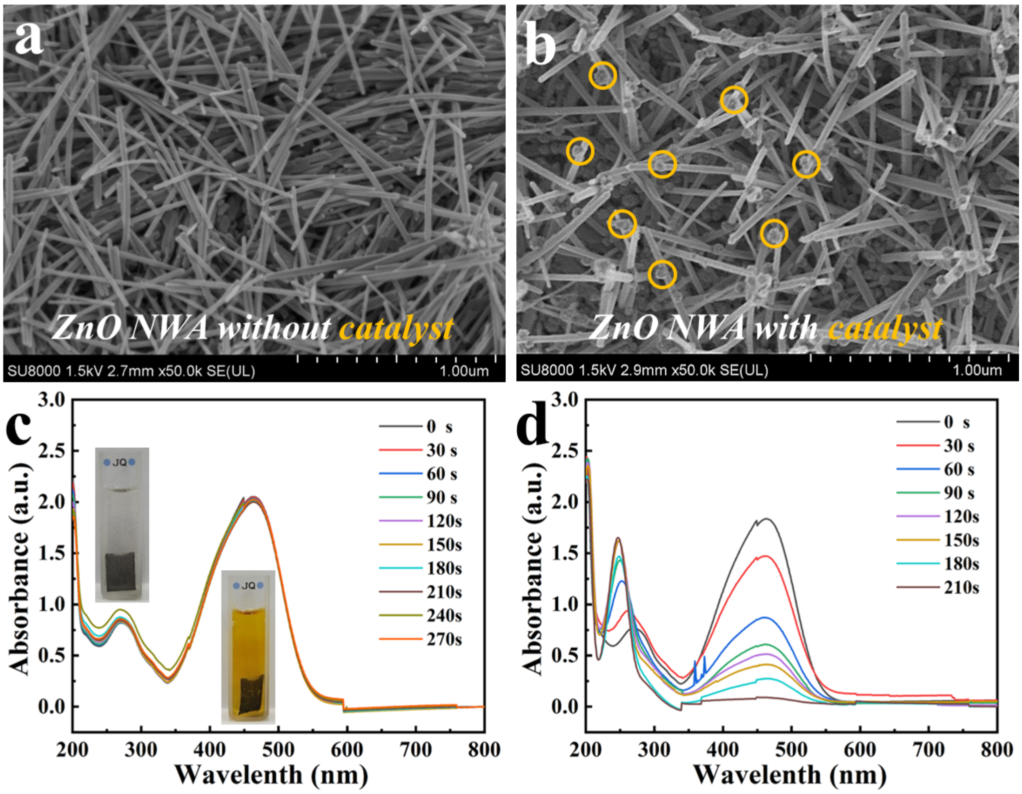

Figure S15. SEM images of ZnO NWA (a) and ZnO NWA-supported Cu nanoparticles (b), UV-vis spectra during the catalytic hydrogenation reaction of MO solutions over the ZnO NWA before (c) and after (d) decoration of Cu nanoparticles.

Figure S16. The digital photographs of ZnO NWAs grown on stainless steel mesh with different shape and size.

Table S1. A summary of Zn coating performances deposited at different current density for 8 min.

Property	Current density (A dm^{-2})			
	3	6	9	12
Grain size (nm)	25.33	20.06	13.59	10.98
Thickness (μm)	13.47	17.50	20.48	30.55
Electrical resistance (mΩ)	10.36	9.84	7.52	4.75

Table S2. Textural characteristics of stainless steel mesh before and after coating with ZnO NWA.

Sample	Porosity	Bulk density	Apparent density	Average pore diameter	Median pore diameter (volume)	Median pore diameter (area)	Total intrusion volume	Total pore area
	%	g ml^{-1}	g ml^{-1}	nm	nm	nm	ml g^{-1}	m^2 g^{-1}
Stainless steel mesh	83.7969	1.2878	7.9479	244935.97	369232.82	183453.93	0.6507	0.011
ZnO NWA	74.2717	1.4603	5.6759	54782.80	395928.96	418.85	0.5086	0.037

Table S3. Comparisons of preparation time and optical performance for the as-prepared sample with previously reported ZnO NWAs grown from different ZnO seed layers via hydrothermal treatment.

Preparation method of seed layer	Time	Optical performance of ZnO NWAs			Ref.
		Wire diameter (nm)	PL emission (nm)	Band gap (eV)	
Magnetron sputtering	5~20 h	30~70	393	-	[3]
Spin coating	2.5~8 h	50~300	378	3.29	[4]
Laser deposition	>6.5 h	20~40	~377	-	[5]
Sol-gel	>4.5 h	47~70	~380	3.18~3.20	[6]
Electrodeposition	**10 min**	**~38.6**	**390**	**3.15**	**Present**

Table S4. Comparisons of preparation time and optical performance for the as-prepared sample with previously reported ZnO NWAs produced by other vapor or liquid phase methods.

Preparation method of ZnO NWAs	Time	Optical performance			Ref.
		Wire diameter (nm)	PL emission (nm)	Band gap (eV)	
Chemical vapor deposition	45 min†	33~83	380	-	[7]
Laser deposition	~2.2 h	30~50	~379	~3.27	[8]
Thermal oxidation	~12 h	40~80	-	3.2~3.3	[9]
Magnetron sputtering	2 h	40	-	3.37	[10]
Vapor transport	30 min†	40~70	~380	-	[11]
Physical vapor deposition	10 h	60	~379	3.27	[12]
Molecular-beam epitaxy	2 h	10~40	375	-	[13]
Chemical bath deposition	3 h	160~580	-	-	[14]
Template electrodeposition	38~65 h	15~90	515	-	[15]
O_2-assisted electrodeposition	42~312 min	140~500	-	-	[16]
Electrochemical anodization	65~80 min	93~105	~400	3.19	[17]
Microwave hydrothermal	**10 min**	**~38.6**	**390**	**3.15**	**Present**

Note: the symbol † represents that the preparation time is exclusive of seed layer or catalytic layer.

References

[1] Morrison S R. Electrochemistry at Semiconductor and Oxidized Metal Electrodes. Plenum Press, New York, 1980, pp. 127-128.

[2] Elliott R J. Intensity of Optical Absorption by Excitons. Physical Review, 1957, 108: 1384-1389.

[3] Zhang W D. Growth of ZnO nanowires on modified well-aligned carbon nanotube arrays. Nanotechnology, 2006, 17(4): 1036.

[4] Greene L E, Law M, Goldberger J, et al. Low-temperature wafer-scale production of ZnO nanowire arrays. Angewandte Chemie, 2003, 115(26): 3139-3142.

[5] Sun Y, Ndifor-Angwafor N G, Riley D J, et al. Synthesis and photoluminescence of ultra-thin ZnO nanowire/nanotube arrays formed by hydrothermal growth. Chemical Physics Letters, 2006, 431(4-6): 352-357.

[6] Lu Y J, Liu C F, Hu C C, et al. Fabrication and characterization of ZnO nanowires array electrodes with high photocurrent densities: Effects of the seed layer calcination time. Materials Chemistry and Physics, 2017, 189: 56-63.

[7] Navarrete E, Güell F, Martinez-Alanis P R, et al. Chemical vapour deposited ZnO nanowires for detecting ethanol and NO_2. Journal of Alloys and Compounds, 2022, 890: 161923.

[8] ElZein B, Yao Y, Barham A S, et al. Toward the growth of self-catalyzed ZnO nanowires perpendicular to the surface of silicon and glass substrates, by pulsed laser deposition. Materials, 2020, 13(19): 4427.

[9] Florica C, Preda N, Costas A, et al. ZnO nanowires grown directly on zinc foils by thermal oxidation in air: Wetting and water adhesion properties. Materials Letters, 2016, 170: 156-159.

[10] Guo Z, Zhao D, Liu Y, et al. Visible and ultraviolet light alternative photodetector based on ZnO nanowire/n-Si heterojunction. Applied Physics Letters, 2008, 93(16): 163501.

[11] Huang M H, Wu Y, Feick H, et al. Catalytic growth of zinc oxide nanowires by vapor transport. Advanced Materials, 2001, 13(2): 113-116.

[12] Kong Y C, Yu D P, Zhang B, et al. Ultraviolet-emitting ZnO nanowires synthesized by a physical vapor deposition approach. Applied Physics Letters, 2001, 78(4): 407-409.

[13] Heo Y W, Varadarajan V, Kaufman M, et al. Site-specific growth of ZnO nanorods using catalysis-driven molecular-beam epitaxy. Applied Physics Letters, 2002, 81: 3046-3048.

[14] Lausecker C, Salem B, Baillin X, et al. Chemical bath deposition of ZnO nanowires using copper nitrate as an additive for compensating doping. Inorganic Chemistry, 2021, 60: 1612-1623.

[15] Li Y, Meng G W, Zhang L, et al. Ordered semiconductor ZnO nanowire arrays and their photoluminescence properties. Applied Physics Letters, 2000, 76: 2011-2013.

[16] Pauporte T, Bataille G, Joulaud L, et al. Well-aligned ZnO nanowire arrays prepared by seed-layer-free electrodeposition and their cassie-wenzel transition after hydrophobization. Journal of Physical Chemistry C, 2009, 114: 194-202.

[17] Tantray A M, Shah M A. Photo electrochemical ability of dense and aligned ZnO nanowire arrays fabricated through electrochemical anodization. Chemical Physics Letters, 2020, 747: 137346.